Production of HNC from the CH($X^2\Pi$) + NH($X^3\Sigma^-$) reaction: Direct dynamics study

Kenta Takahashi, Toshiyuki Takayanagi*

Department of Chemistry, Saitama University, 255 Shimo-Okubo, Sakura-ku, Saitama City, Saitama 338-8570, Japan

Abstract

The production mechanism and dynamics of the HNC molecule from the radical-radical CH + NH reaction on the lowest doublet potential energy surface has been theoretically studied using electronic structure calculations. We have applied a direct dynamics simulation technique at the B3LYP/6-311++G (d, p) level of theory. The accuracy of the B3LYP-level potential energy surface was systematically confirmed from the comparison to more accurate MRCI-level and CCSD(T)-level calculations. More than 250 classical trajectories were integrated and we have found that the CH + NH reaction somewhat favors the HNC + H production channel over the HCN + H production despite that the energy level of HCN + H is lower than that of HNC + H. Detailed reaction mechanisms will be discussed on the basis of the trajectory results.

---

* Corresponding author. *E-mail address*: tako@chem.saitama-u.ac.jp (T. Takayanagi)

1. Introduction

Despite its thermochemical instability, hydrogen isocyanide (HNC) has been frequently detected in many interstellar clouds and understanding of the anomalous abundance ratio of HNC/HCN observed in astrophysical environments has been an important issue from a viewpoint of astrochemistry as well as physical chemistry [1-5]. So far, it has been generally accepted that the $HCNH^+$ cation is the major precursor of the HCN/HNC production since it is known that this cation recombines with an electron to reach both H + HCN and H + HNC channels with the branching ratio being nearly unity [6-10].

Very recently, we have started a research project studying neutral-neutral chemical reactions that finally produce the HCN/HCN molecules from a theoretical point of view. We have reported that the $C(^3P)$ + $NH_2(^2B_1)$ [11] and $C_2(X^1\Sigma_g^+)$ + $NH(X^3\Sigma^-)$ [12] reactions proceed without barriers and produce the HNC molecule with relatively large yields. It should be emphasized that these two reactions are radical-radical type reactions, which are generally difficult to be studied experimentally due to the difficulty in producing enough radical concentrations under gas phase experimental conditions. It is then difficult to determine product branching ratio for such radical-radical reactions from an experimental side. On the other hand, it should be mentioned that theoretical studies based on modern electronic structure calculations and reaction dynamics calculations would be quite useful especially for such chemical reactions.

In our previous studies on the $C(^3P)$ + $NH_2(^2B_1)$ and $C_2(X^1\Sigma_g^+)$ + $NH(X^3\Sigma^-)$ reactions [11,12], we have employed direct dynamics methods combined with the density-functional formalism, where classical trajectories are directly calculated using derivatives obtained from electronic structure calculations. In order to simulate interstellar chemical reactions, collision energies were set to nearly zero since interstellar reactions generally occur under extremely low temperature conditions. We have found that features of the potential energy surface in entrance regions play a very important role in determining collisional orientations for such low-energy collision conditions. Another important conclusion derived from our previous studies is that reaction dynamics itself plays an significant role in determining product branching ratios because the system has a large excess energy above final product

energy levels. Notice that radical-radical type reaction systems generally have a large excess energy due to chemical bond formation. In this case, the lifetime of reaction intermediates on the potential energy surface becomes relatively short. We have found that the $C_2(X^1\Sigma_g^+)$ + $NH(X^3\Sigma^-)$ reaction is exactly the case and leads to the C + HNC product channel with a very high efficiency. This result implies that statistical approximations such as RRKM cannot be used to obtain product branching ratios at least for this kind of chemical reactions.

In this paper, we extend our previous studies and apply the reaction dynamics method to the $CH(X^2\Pi)$ + $NH(X^3\Sigma^-)$ reaction. As far as we are aware, the contribution of the $CH(X^2\Pi)$ + $NH(X^3\Sigma^-)$ reaction to the HNC production has not yet been studied from the experimental side nor theoretical side although the potential energy surface for the [H_2,C,N] system has been previously studied using various electronic structure methods [11,13-16]. As will be shown later, the energy level of the $CH(X^2\Pi)$ + $NH(X^3\Sigma^-)$ reactants is much larger than those of reaction intermediates on the lowest doublet potential energy surface. This also suggests that dynamics calculations should be performed for understanding an overall mechanism of this reaction.

2. Computational method

Geometries of reactants, products, intermediates, and transition-states on the lowest doublet potential energy surface for the $CH(X^2\Pi)$ + $NH(X^3\Sigma^-)$ reaction have been optimized using the hybrid density-functional B3LYP method [17,18] with the 6-311++G(d, p) basis set. Harmonic vibrational frequencies were calculated at the same level of theory in order to characterize the optimized geometries as potential minima or transition states as well as to obtain zero-point energy corrections. In order to obtain more accurate relative energies, we have performed single-point energy calculations at the CCSD(T)/6-311++G(3df,3pd) and full-valence MRCI/cc-pVTZ levels of theory. The molecular orbitals used in the MRCI calculation were obtained from the CASSCF calculation where 11 electrons were distributed among 10 active orbitals. All calculations were carried out using the Gaussian 03 [19] and Molpro 2002 [20] package programs.

We have performed on-the-fly direct trajectory calculations on the lowest doublet potential energy surface for the CH + NH reaction. The direct trajectory calculations were carried out at the B3LYP/6-311++G(d, p) level, which was determined by compromise of computational costs and the accuracy. We employed the BOMD (Born-Oppenheimer molecular dynamics) method implemented in the GAUSSIAN 03 package [19]. This method uses a fifth-order polynomial fitted to the energy, gradient, and Hessian at each time step, and then the step size is taken to be much larger than the step size used in the normal method employing only the gradient information [21]. As will be shown below, B3LYP/6-311++G(d, p)-level potential energy curves as a function of an appropriate internal coordinate were compared to the potential curves obtained at the MRCI/cc-pVTZ level of theory in order to confirm the validity to use the B3LYP potential energy surface for dynamics calculations.

3. Results and discussion

Fig. 1 shows the overall potential energy diagram for the $CH(X^2\Pi)$ + $NH(X^3\Sigma^-)$ reaction on the lowest doublet potential energy obtained at the B3LYP/6-311++G(d, p) level of theory. In this figure, the energy level for the HNC + H channel is defined to be zero. Table 1 summarizes relative energies of reactants, products, intermediates and transition states used in Fig. 1. The accuracy of the energy levels of the present electronic structure calculations was checked by comparing those to thermochemical data [22] for the CH + NH, $C(^3P)$ + $NH_2(^2B_1)$, $N(^4S)$ + $CH_2(^3B_1)$, and H + HCN channels. It was found that the present B3LYP calculations are in agreement with the corresponding experimental data within ± 5 kcal/mol. The most important point found from Fig. 1 is that the $CH(^2\Pi)$ + $NH(^3\Sigma)$ reactant energy level is quite high on the potential energy surface. This indicates that the system has a large excess energy, thus leading to short lifetime of reaction intermediates.

Fig. 2 displays potential energy curves in the entrance region for the CH + NH approaches calculated at the MRCI level of theory. Three types of geometrical approaches were examined. Fig. 2a shows the potential curve as a function of the CN internuclear

distance with other internal coordinates being optimized with respect to energy. It is seen that the reaction of CH with NH leads to the *trans*-HCNH intermediate without an entrance barrier. This is a very important point from a viewpoint of interstellar chemistry. We have also found that CH + NH leads to *cis*-HCNH without a barrier though the corresponding potential energy curve is not shown. Fig. 2b and 2c display the potential energy curves for two collinear approaches of CH + NH as a function of the NH and CH distances, respectively. The result indicates that there exist shallow hydrogen-bonding potential wells in the entrance regions. The MRCI calculation has given a somewhat deeper well for NH···CH compared to the potential well for CH···NH. Fig. 2 also includes potential energy curves calculated at the B3LYP/6-311++G(d, p) level of theory in order to demonstrate the validity to use the B3LYP potential energy surface in dynamics calculations. The agreement between the MRCI and B3LYP results is found to be reasonable.

Fig. 3 shows potential energy curves similar to Fig. 2 but for two exit channels: *trans*-HNCH $\rightarrow$ H + HCN and *trans*-HCNH $\rightarrow$ H + HNC. It is interesting to note that the HNCH $\rightarrow$ H + HCN process has a small exit barrier due to production of a triple bond in the HCN molecule. It is seen that the HNCH $\rightarrow$ H + HNC dissociation process also has a very low exit barrier. We can see that the B3LYP method slightly underestimates these exit barriers compared to the MRCI result; however, since the CH + NH collision system has a large excess energy, it is expected that these differences do not largely affect dynamics results.

It should be important to give a comment on the reasonable agreement between the MRCI and B3LYP potential energy curve since the B3LYP method is a single reference method. The agreement may be somewhat fortuitous; however, notice that the spin state of the lowest potential energy surface of the CH + NH reaction system is doublet and then the spin-unrestricted method (UB3LYP) was employed in this study. It is generally known that the spin-unrestricted method sometimes can describe properly the asymptotic region of the potential energy surface although the so-called spin-contamination may be large in such regions. In fact, we have noticed that the spin-contamination is somewhat significant especially in the CH($^2\Pi$) + NH($^3\Sigma$) asymptotic region. We have also confirmed that the spin-contamination is not so important in the H + HCN/HNC asymptotic regions. In any case, it should be emphasized that the detailed comparison of the low-level potential surface

to accurate high-level results should be performed prior to dynamics calculations.

Now, let us present results of BOMD calculations for the CH + NH reaction. In the BOMD calculations, the initial distance between CH and NH was set 4-5 Å and the initial internuclear distances of CH and NH were set to their equilibrium distances. The vibrational energies of CH and NH were completely ignored for computational simplicity. It should be emphasized that this condition is somewhat unrealistic but its effect is expected to be small due to a very large available energy for this reaction system. The relative translational energy was fixed to nearly zero (~ 10^{-4} kcal/mol) in order to simulate chemical reactions under interstellar conditions. The initial orientation between CH and NH was randomly chosen. We have generated 257 initial conditions and then run the GAUSSIAN program for each condition. About 250 trajectories obviously do not allow good quality statistical sampling but it must be kept in mind that the computational cost of the direct trajectory calculations is high even at the B3LYP/6-311++G(d, p) level. In spite of this limitation, we believe that the present direct classical trajectory calculations give important information on the reaction dynamics of the CH + NH reaction.

Fig. 4 displays typical snapshots showing the HNC production along the BOMD trajectory. First, the CN bond is formed due to a strong attraction (see Fig. 2a) and then the *trans*-HCNH intermediate is immediately produced. Since this intermediate has a very large internal energy, we can say that this intermediate is in highly vibrational state. After several periods of CN vibrations, it is seen that the *cis*-HCNH intermediate is then produced via bending motion. However, the HNC + H products are readily formed after this. The overall reaction time of this trajectory is about 500 fs. This reaction pathway presented in Fig. 4 can easily be understood from the energy diagram of Fig. 1.

Interestingly, we have found that the HCN + H production dynamics is different from the mechanism of the HNC + H production presented in Fig. 4. The typical snapshots for the HCN + H production dynamics are shown in Fig. 5. In an early stage of this trajectory, the HCNH intermediate (*trans*- and *cis*-) is formed but it isomerizes into the H_2CN intermediate through the corresponding transition state (TS6 in Fig. 1). Once the H_2CN intermediate is formed, it dissociates into the HCN + H channel within ~ 100 fs. This is simply because the H_2CN intermediate cannot dissociate into the HNC + H channel.

Fig. 6 shows the snapshots of the CN + H_2 production dynamics although its overall contribution was found to be very small. In the trajectory of Fig. 6a, H_2 + CN is formed from the *cis*-HCNH intermediate via a H_2 elimination mechanism, while in Fig. 6b the dissociating hydrogen atom abstracts the other hydrogen atom in the HCN molecule. These unusual mechanisms presumably come from the fact that the reaction system has a very large excess energy. However, at the same time, the present dynamics calculations suggest that, if the reaction system has a large energy, the overall reaction mechanism and dynamics cannot be predicted only from the information on the potential energy diagram showing minimum-energy pathways.

Table 1 summarizes the statistical result of the present BOMD calculations for the CH + NH reaction. It was found that 152 trajectories lead to HNC + H implying that the branching fraction of this channel is 59%, while the branching fraction of the HCN + H channel was calculated to be 40 %. From the present BOMD simulation, it is therefore concluded that the HNC molecule is the main product of the CH + NH reaction. We have further analyzed the energy distributions for both HNC + H and HCN + H channels in order to understand the reaction dynamics more quantitatively. Fig. 7a displays the relative translational energy distributions for the HNC + H and HCN + H channels. The distributions has peaks at ~ 0 kcal/mol, showing a typical distribution for reactions with no exit barrier. However, it is seen that the distribution of HNC + H shows larger population for low transitional energy compared to the result of the HCN + H channel. This is reasonable since the HCN + H products are mainly formed in the dissociation of the H_2CN intermediate. Notice that the $H_2CN \rightarrow$ H + HCN dissociation process has a small exit barrier of ~ 4 kcal/mol. Fig. 7b displays the vibrational energy distributions of the HCN and HNC molecules produced in the CH + NH reaction. It is seen that a large part of the available energy is partitioned into the vibrational energies of HCN and HNC. This indicates that the produced HCN/HNC molecules are in highly vibrational states.

It should be emphasized that the calculated HCN/HNC branching fraction is only qualitative since the branching fraction was obtained from classical mechanical calculations [11]. As shown in Fig. 7, it is seen that HCN/HNC molecules have an enough vibrational energy for the HCN $\leftrightarrow$ HNC isomerization since the corresponding isomerization barrier

height from HNC to HCN is 33 kcal/mol [23]. In the present BOMD calculations, we have further integrated the trajectories for 0.5-1.0 ps even after the H + HCN/HNC production. In fact, we have seen a few trajectories showing the HCN ↔ HNC isomerization within the present simulation time. Of course, it would be possible to perform long-time simulations in order to understand the energy partitioning into vibrational modes of HCN/HCN. This is an important issue which should be addressed in the near future; however, notice that the dynamics is still based on classical mechanics. Presumably, state-to-state quantum dynamics methods including vibrational quantization in HCN/HNC should be performed in order to obtain reliable branching fractions. This point has been previously discussed in somewhat detail in our previous studies on the C + NH_2 [11] and C_2 + NH [12] reactions. In spite of these limitations, we believe that the present BOMD simulations give an important insight into the HCN/HNC production mechanism and dynamics in the radical-radical CH + NH reaction.

4. Conclusions

In this work we have applied the direct dynamics simulation method to the radical-radical CH($X^2\Pi$) + NH($X^3\Sigma^-$) reaction to understand the importance of the HNC production. In order to save computational time, we have employed the hybrid density-functional method at the B3LYP level of theory in the direct dynamics calculations. In spite of less computational time for the B3LYP method, we have shown that the B3LYP potential energy surface is accurate enough to be used in the on-the-fly dynamics calculations by comparing it with more accurate MRCI potential energy surface. We think that this comparison is a very important step for direct dynamics simulations for obtaining reliable computational results. It was found that the HNC + H channel is the main product channel of the CH + NH reaction although a large amount of the available energy is partitioned into vibrations of the product HNC molecule. Notice that the calculated HCN/HNC branching fraction is only qualitative since the dynamics is based on purely classical mechanics.

We have demonstrated that the direct dynamics simulation technique is quite useful

for understanding the product branching in simple chemical reactions. In particular, in the case of radical-radical chemical reaction, the reaction system generally has a large excess energy on the potential energy surface. Therefore, this tentatively leads to relatively short lifetimes of reaction intermediates and thus the application of the direct dynamics method would make more practical. As mentioned in Introduction, radical-radical reactions are generally difficult to be studied experimentally since the concentration of the reactant radicals should be high enough for spectroscopic detection. In addition, it is generally accepted that the determination of product branching in chemical reactions is more difficult than rate coefficient (cross section) measurements. It should be emphasized that the understanding of the mechanism and dynamics of various radical-radical reactions is very important in the fields of interstellar chemistry as well as combustion chemistry. We hope that the present theoretical study stimulates further experimental developments.

Acknowledgement

This work was partly supported by the Grant-in-Aid for Scientific Research of the Ministry of Education, Culture, Sports, Science, and Technology of Japan (Grant No. 17550007).

References

[1] W. M. Irvine, F. P. Schloeb, Astrophys. J. 282 (1984) 516.

[2] A. Wooten, N. J. Evans, II, R. Snell, P. V. Bout, Astrophys. J. 225 (1978) L143.

[3] T. Hirota, S. Yamamoto, H, Mikami, M. Ohishi, Astrophys. J. 503 (1998) 717.

[4] C. M. Walmsley, J. Chem. Soc. Faraday Trans. 89 (1993) 2119.

[5] J. Semaniak, B. F. Minaev, A. M. Derkatch, F. Hellberg, A. Neau, S. Rosén, R. Thomas, M. Larsson, H. Danared, A. Paál, M. af Ugglas, Astrophys. J. Suppl. 135 (2001) 275.

[6] Y. Shiba, T. Hirano, U. Nagashima, K. Ishii, J. Chem. Phys. 108 (1998) 698.

[7] T. Taketsugu, A. Tajima, K. Ishii, T. Hirano, Astrophys. J. 608 (2004) 323.

[8] K. Ishii, A. Tajima, T. Taketsugu, K. Yamashita, Astrophys. J. 636 (2006) 927.

[10] H. Tachikawa, Phys. Chem. Chem. Phys. 1 (1999) 4925.

[11] T. Takayanagi, T. Taketsugu, Chem. Phys. Lett. 417 (2006) 143.

[12] K. Takahashi, T. Takayanagi, Chem. Phys. Lett. 429 (2006) 399.

[13] M. ter Horst, G. C. Schatz, L. B. Harding, J. Chem. Phys. 105 (1996) 558.

[14] R. Sumathi, M. T. Nguyen, J. Phys. Chem. A 102 (1998) 8013.

[15] S. Petrie, Icarus, 151 (2001) 196.

[16] S. Petrie, J. Phys. Chem. A, 106 (2002) 11181.

[17] A. D. Becke, J. Chem. Phys. 98 (1993) 5648.

[18] C. Lee, W. Yang, R. G. Parr, Phys. Rev. B 37 (1988) 785.

[19] M. J. Frisch, G. W. Trucks, H. B. Schlegel, G. E. Scuseria, M. A. Robb, J. R. Cheeseman, J. A. Montgomery, Jr., T. Vreven, K. N. Kudin, J. C. Burant, J. M. Millam, S. S. Iyengar, J. Tomasi, V. Barone, B. Mennucci, M. Cossi, G. Scalmani, N. Rega, G. A. Petersson, H. Nakatsuji, M. Hada, M. Ehara, K. Toyota, R. Fukuda, J. Hasegawa, M. Ishida, T. Nakajima, Y. Honda, O. Kitao, H. Nakai, M. Klene, X. Li, J. E. Knox, H. P. Hratchian, J. B. Cross, C. Adamo, J. Jaramillo, R. Gomperts, R. E. Stratmann, O. Yazyev, A. J. Austin, R. Cammi, C. Pomelli, J. W. Ochterski, P. Y. Ayala, K. Morokuma, G. A. Voth, P. Salvador, J. J. Dannenberg, V. G. Zakrzewski, S. Dapprich, A. D. Daniels, M. C. Strain, O. Farkas, D. K. Malick, A. D. Rabuck, K. Raghavachari, J. B. Foresman, J. V. Ortiz, Q. Cui, A. G. Baboul, S. Clifford, J. Cioslowski, B. B. Stefanov, G. Liu, A. Liashenko, P. Piskorz, I. Komaromi, R. L. Martin, D. J.

Fox, T. Keith, M. A. Al-Laham, C. Y. Peng, A. Nanayakkara, M. Challacombe, P. M. W. Gill, B. Johnson, W. Chen, M. W. Wong, C. Gonzalez, and J. A. Pople, Gaussian 03, Revision C.02, Gaussian, Inc., Wallingford CT, 2004.

[20] MOLPRO, a package of ab initio programs, H.-J. Werner and P. J. Knowles, version 2002.1, R. D. Amos, A. Bernhardsson, A. Berning, P. Celani, D. L. Cooper, M. J. O. Deegan, A. J. Dobbyn, F. Eckert, C. Hampel, G. Hetzer, P. J. Knowles, T. Korona, R. Lindh, A. W. Lloyd, S. J. McNicholas, F. R. Manby, W. Meyer, M. E. Mura, A. Nicklass, P. Palmieri, R. Pitzer, G. Rauhut, M. Schütz, U. Schumann, H. Stoll, A. J. Stone, R. Tarroni, T. Thorsteinsson, and H.-J. Werner.

[21] J. M. Millam, V. Bakken, W. Chen, W. L. Hase, B. H. Schlegel, J. Chem. Phys. 111 (1999) 3800.

[22] NIST Chemistry Webbook (http://www.webbook.nist.gov/chemistry/).

[23] J. M. Bowman, B. Gazdy, J. A. Bentley, T. J. Lee, C. E. Dateo, J. Chem. Phys. 99 (1993) 308.

Table 1 Relative energies of reactants, products, intermediates, and transition states for the CH + NH reaction system.

	B3LYP[a]	CCSD(T)[b]	Exp.[c]	ZPE[d]
Reactants or Products				
$CH(^2\Pi) + NH(^3\Sigma^-)$	123.45	124.86	130.19	8.68
$H(^2S) + HNC(^1\Sigma)$	0.0	0.0	0.0	9.85
$H(^2S) + HCN(^1\Sigma)$	-13.99	-14.11	-17.4	10.27
$H_2(^1\Sigma) + CN(^2\Sigma)$	9.19	8.19	2.20	9.38
$NH_2(^2B_1) + C(^3P)$	112.53	113.24	114.98	11.86
$CH_2(^3B_1) + N(^4S)$	105.68	102.48	103.52	10.75
Intermediate				
trans-HCNH	-25.59	-30.98		16.14
cis-HCNH	-31.15	-26.49		15.51
H_2CN	-44.84	-39.14		15.72
H_2NC	-13.88	-9.07		16.45
HN···HC	122.93	123.99		9.13
HC···HN	122.17	123.55		9.74
Transition State				
TS1	123.80	124.87		10.00
TS2	122.56	124.26		9.83
TS3	0.64	1.91		10.07
TS4	-8.71	-4.58		10.63
TS5	23.40	28.01		11.48
TS6	2.42	5.69		12.36
TS7	-21.60	-15.71		14.46
TS8	-22.27	-16.56		14.37
TS9	9.46	13.63		10.89
TS10	0.64	1.91		10.07
TS11	-8.71	-4.59		10.62
TS12	-10.22	-7.98		10.83

[a]All geometries were optimized at B3LYP/6-311++G(d, p) level of theory.

[b]Single-point energies were calculated at the CCSD(T)/6-311++G(3df, 3pd)// B3LYP/6-311++G(d,p) level.

[c]Experimental data are taken from Ref. 22

[d]Zero-point energies were obtained from harmonic frequency analyses at the B3LYP/6-311++G(d, p) level of theory.

Table 2 Result of the BOMD calculations for the CH + NH reaction at the B3LYP/6-311++G(d, p) level of theory.

Product channel	# of Trajectory	Fraction (%)
HNC + H	152	59.1
HCN + H	102	39.7
CN + H_2	3	1.2
Sum	257	100.0

Figure Captions

Fig. 1 Potential energy diagram for the CH($X^2\Pi$) + NH($X^3\Sigma^-$) reaction obtained from the present electronic structure calculations. The relative energies include zero-point corrections obtained from the B3LYP/6-311++G(d, p)-level calculations.

Fig. 2 Comparison of the B3LYP and MRCI potential energy curves as a function of the internal distance for the CH + NH approaches.

Fig. 3 Comparison of the B3LYP and MRCI potential energy curves for (a) *trans*-HCNH $\rightarrow$ H + HCN and (b) *trans*-HCNH $\rightarrow$ H + HNC dissociation processes.

Fig. 4 Typical snapshots of molecular structure along a trajectory showing the HNC + H production from the CH + NH reaction.

Fig. 5 Typical snapshots of molecular structure along a trajectory showing the HCN + H production from the CH + NH reaction.

Fig. 6 Typical snapshots of molecular structure along a trajectory showing the H_2 + CN production from the CH + NH reaction.

Fig. 7 Product energy distributions for the CH + NH $\rightarrow$ HCN/HNC + H reaction: (a) relative translational energy between HCN/HNC and H, (b) internal vibrational energies for the product HCN/HCN molecules. The averaged energy values are also shown.

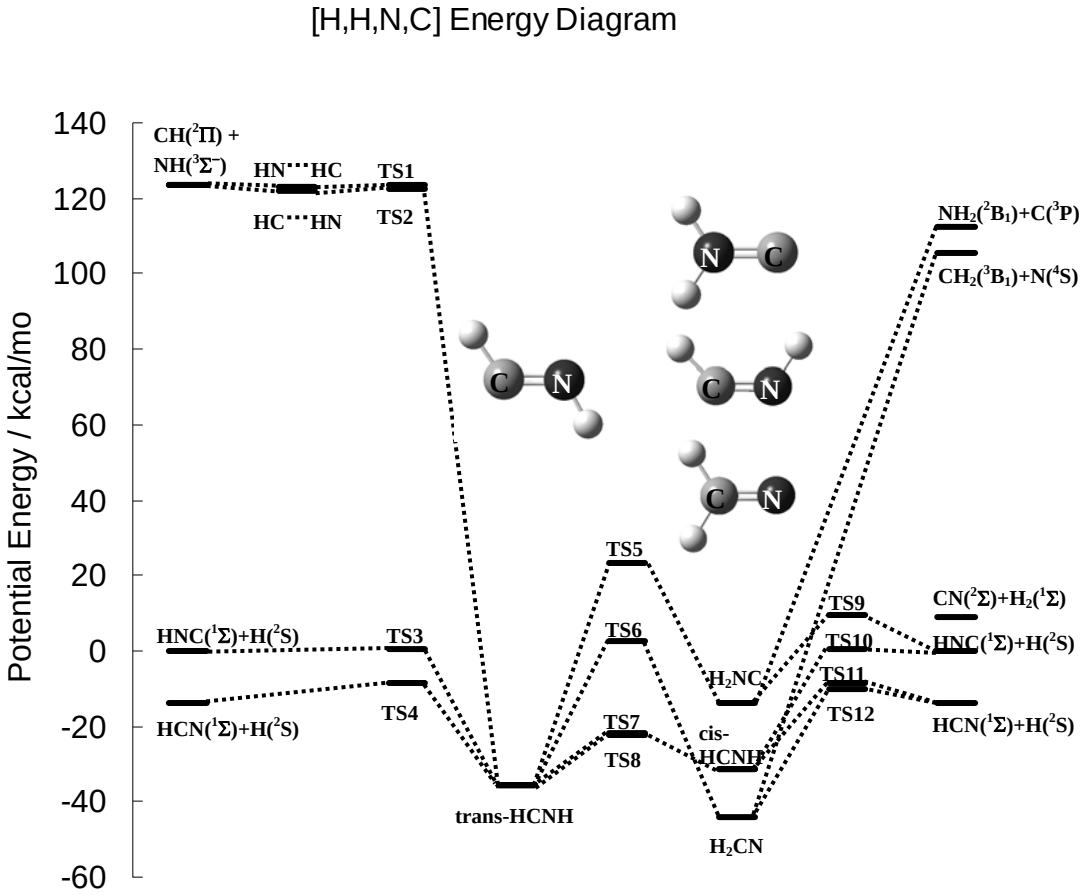
[H,H,N,C] Energy Diagram
Potential Energy / kcal/mo
140
120
100
80
60
40
20
0
-20
-40
-60
CH(2Π) +
NH(3Σ-)
HN···HC
HC···HN
TS1
TS2
HNC(1Σ)+H(2S)
HCN(1Σ)+H(2S)
TS3
TS4
trans-HCNH
TS5
TS6
TS7
TS8
H2NC
cis-HCNH
H2CN
TS9
TS10
TS11
TS12
NH2(2B1)+C(3P)
CH2(3B1)+N(4S)
CN(2Σ)+H2(1Σ)
HNC(1Σ)+H(2S)
HCN(1Σ)+H(2S)

Fig.1

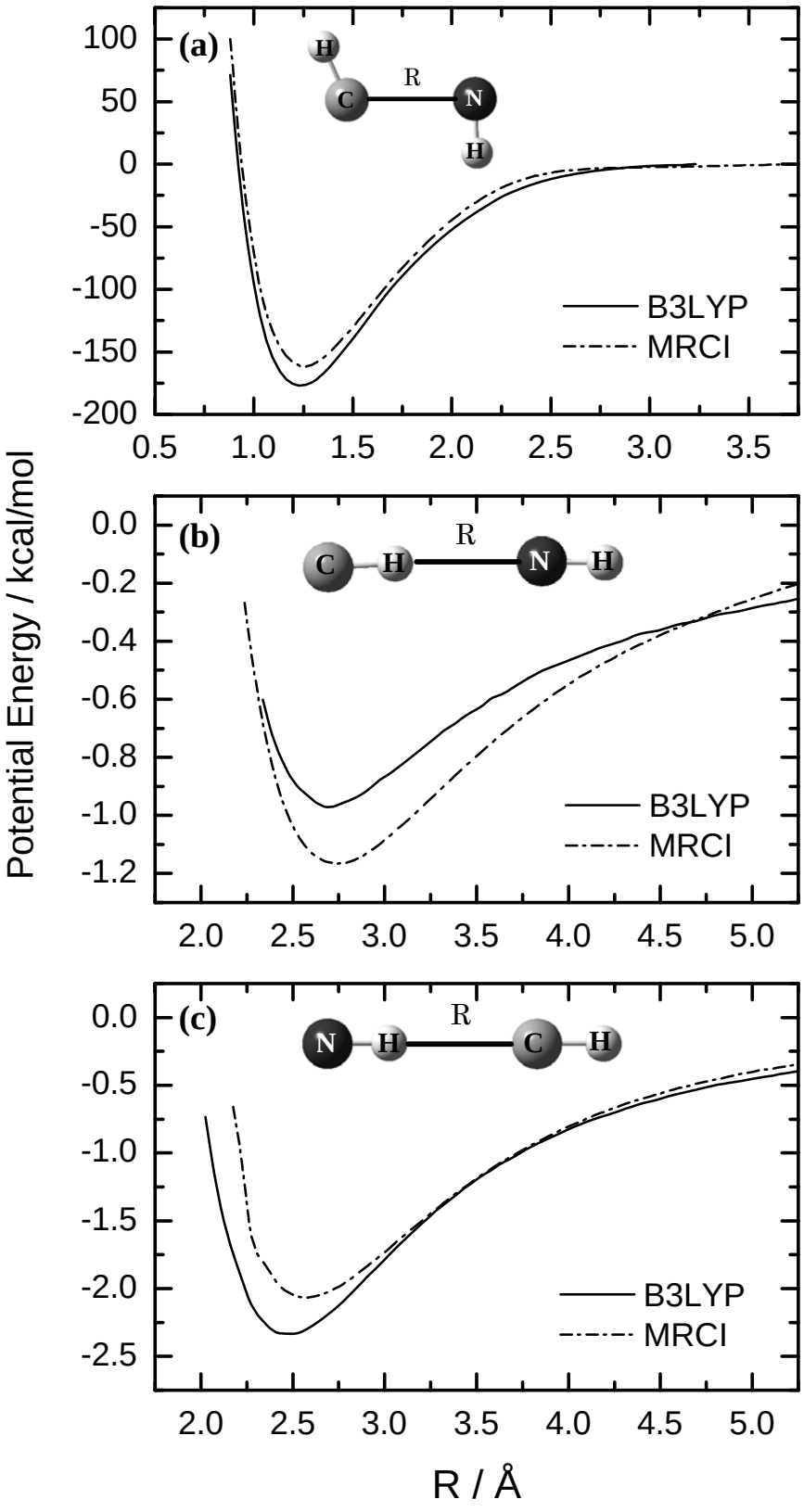
(a)
H
C
R
N
H
B3LYP
MRCI
(b)
C
H
R
N
H
B3LYP
MRCI
(c)
N
H
R
C
H
B3LYP
MRCI
Potential Energy / kcal/mol
R / Å

Fig.2

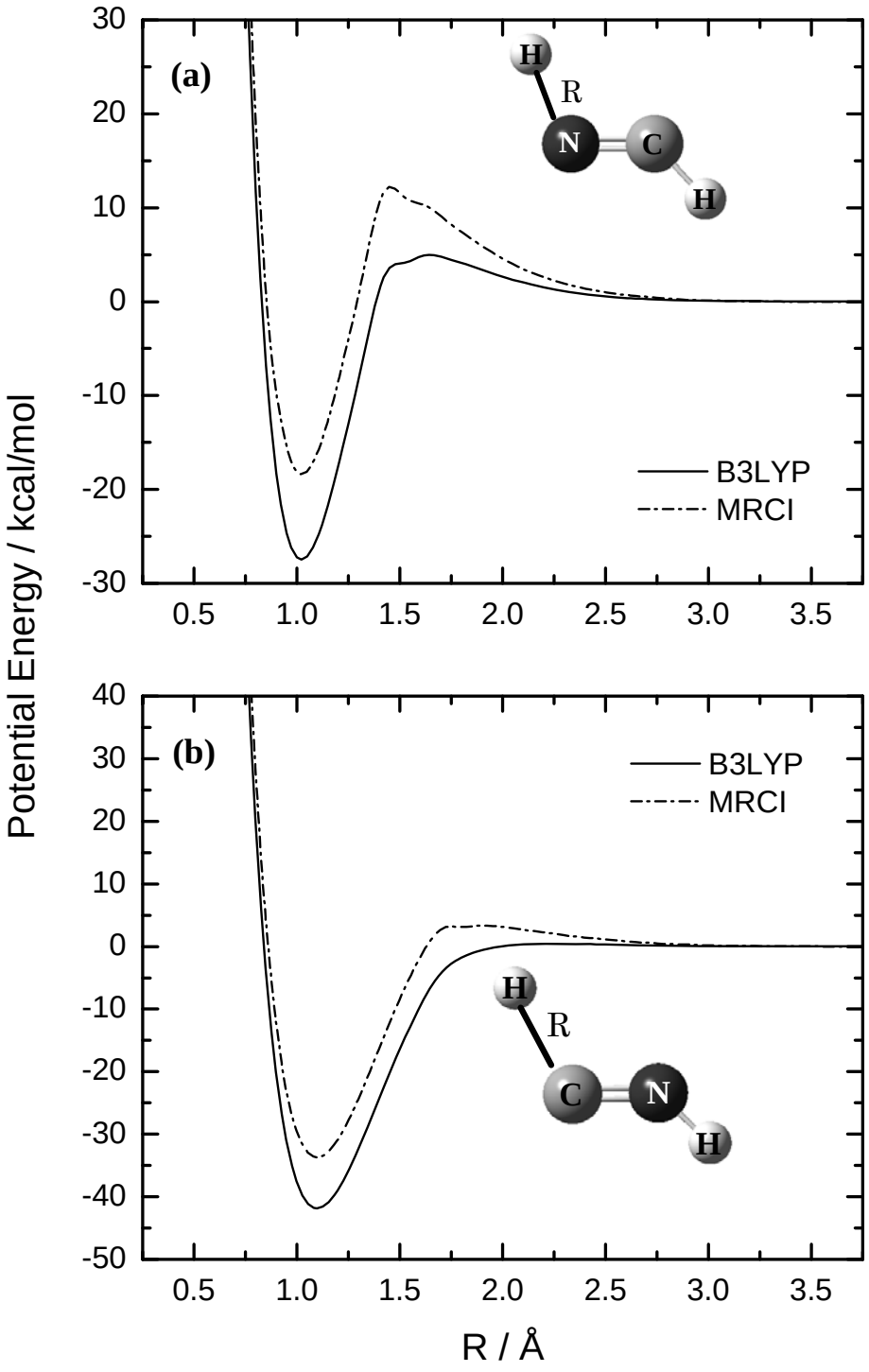
(a)
H
R
N
C
H
B3LYP
MRCI
(b)
B3LYP
MRCI
H
R
C
N
H
Potential Energy / kcal/mol
R / Å

Fig.3

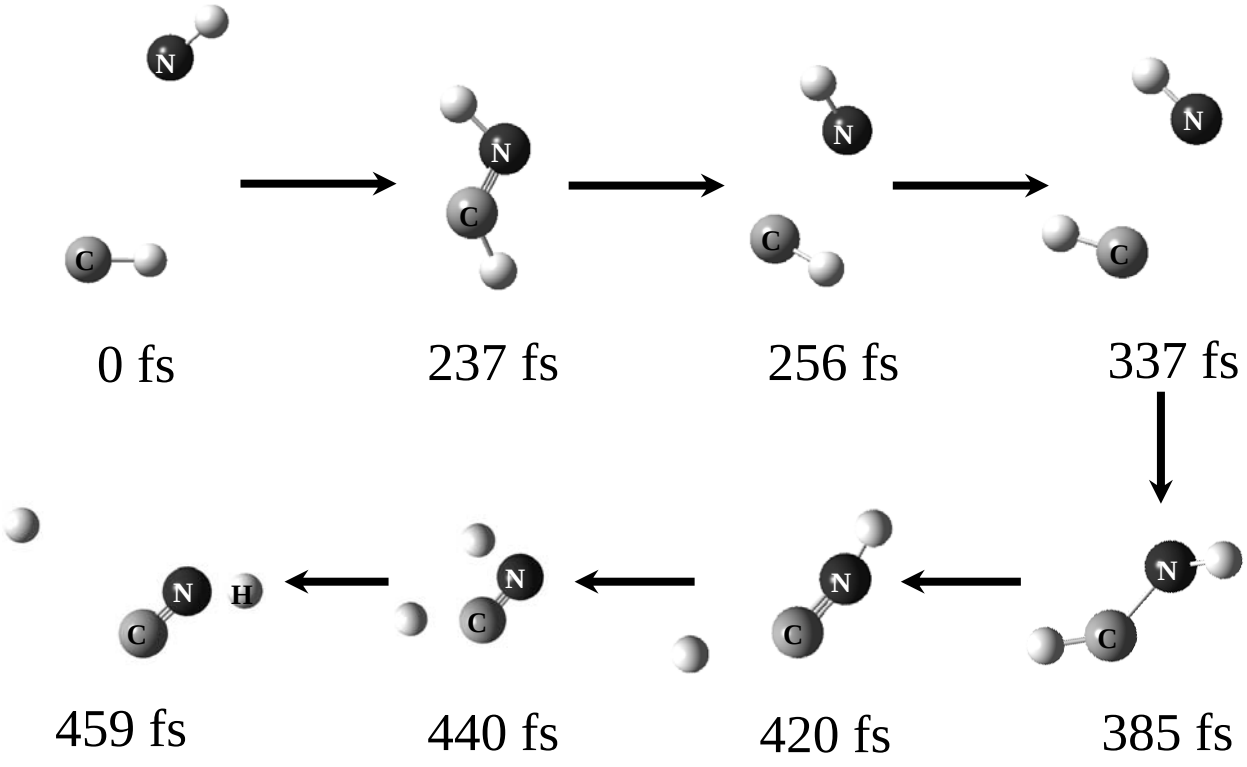

Fig.4

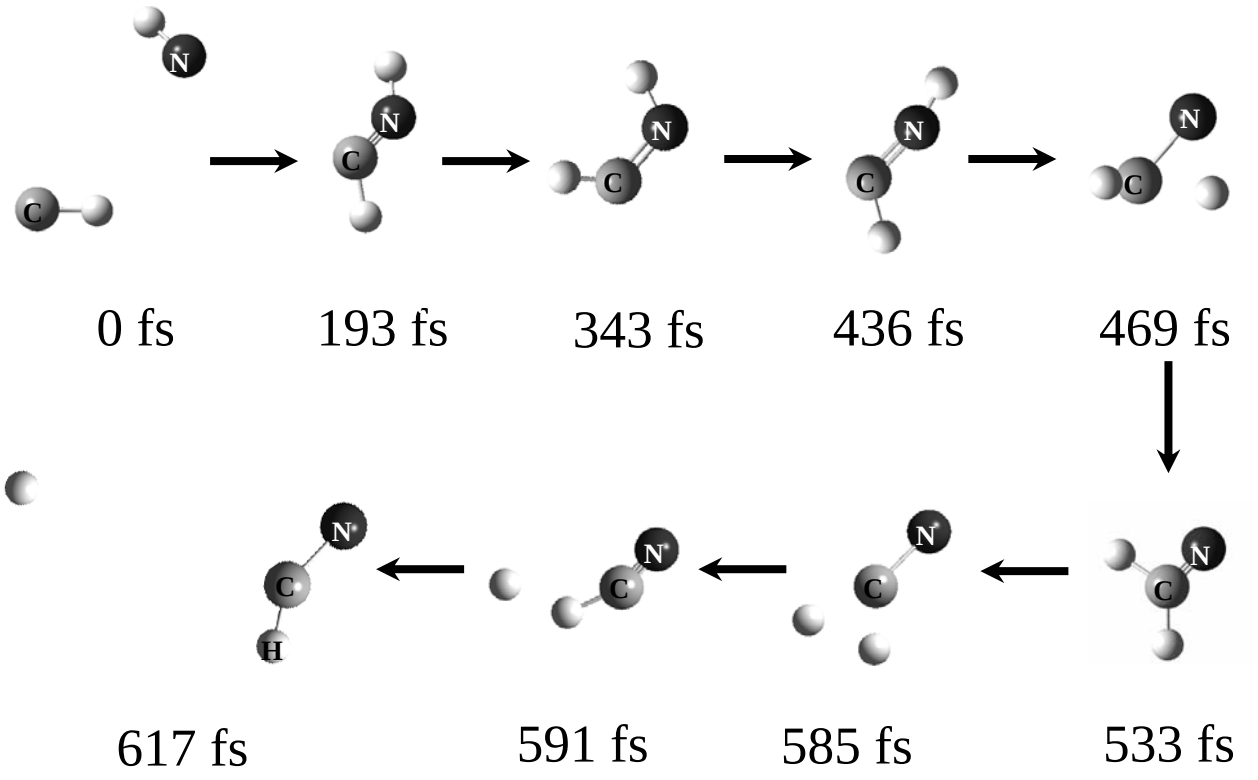
N
C
N
C
N
C
N
C
N
C
0 fs
193 fs
343 fs
436 fs
469 fs
N
C
N
C
N
C
H
533 fs
585 fs
591 fs
617 fs

Fig.5

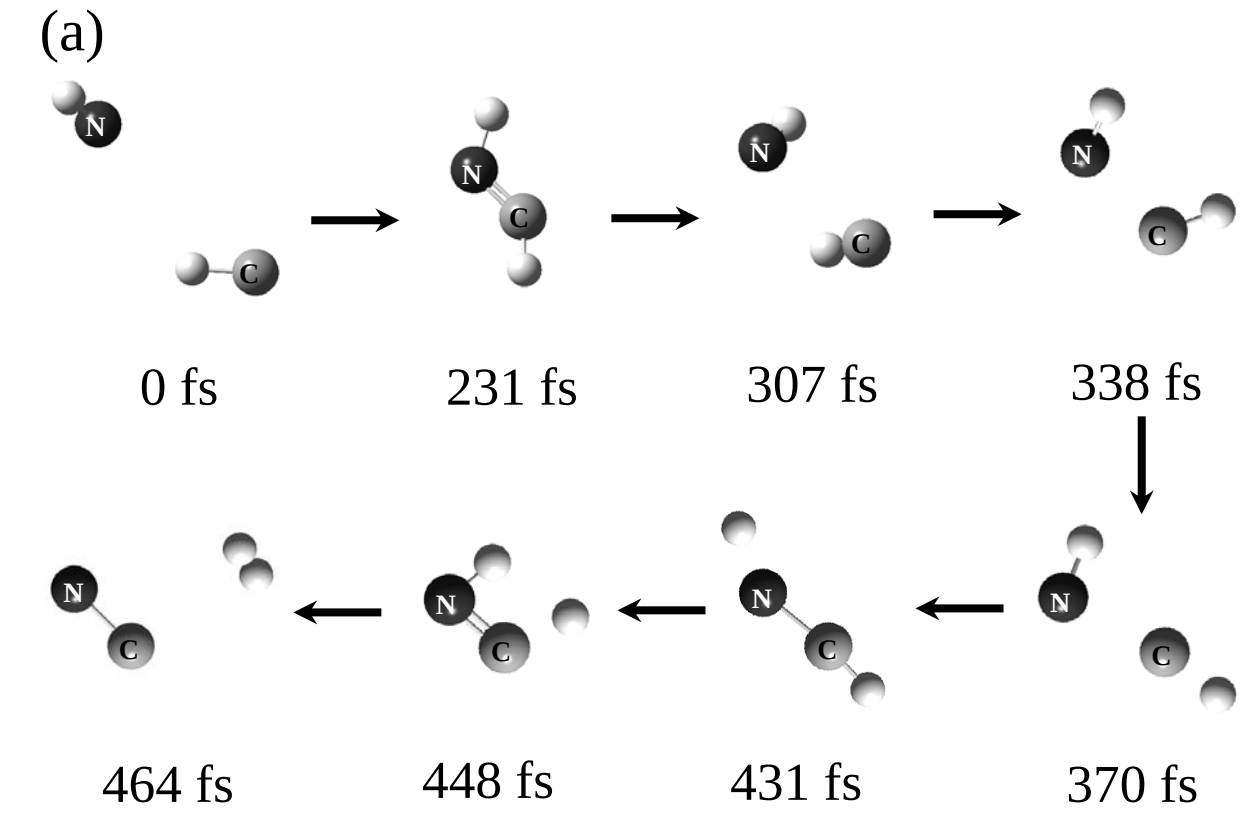
(a)
0 fs
231 fs
307 fs
338 fs
370 fs
431 fs
448 fs
464 fs

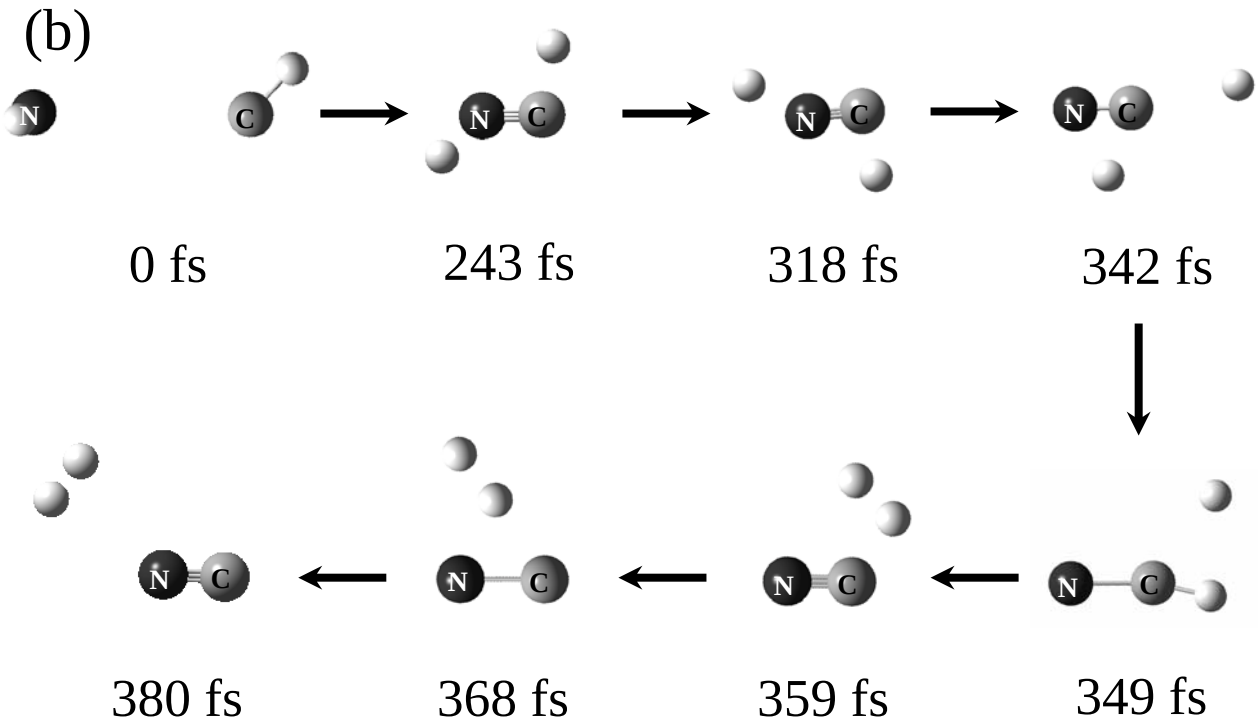
(b)
0 fs
243 fs
318 fs
342 fs
349 fs
359 fs
368 fs
380 fs

Fig.6

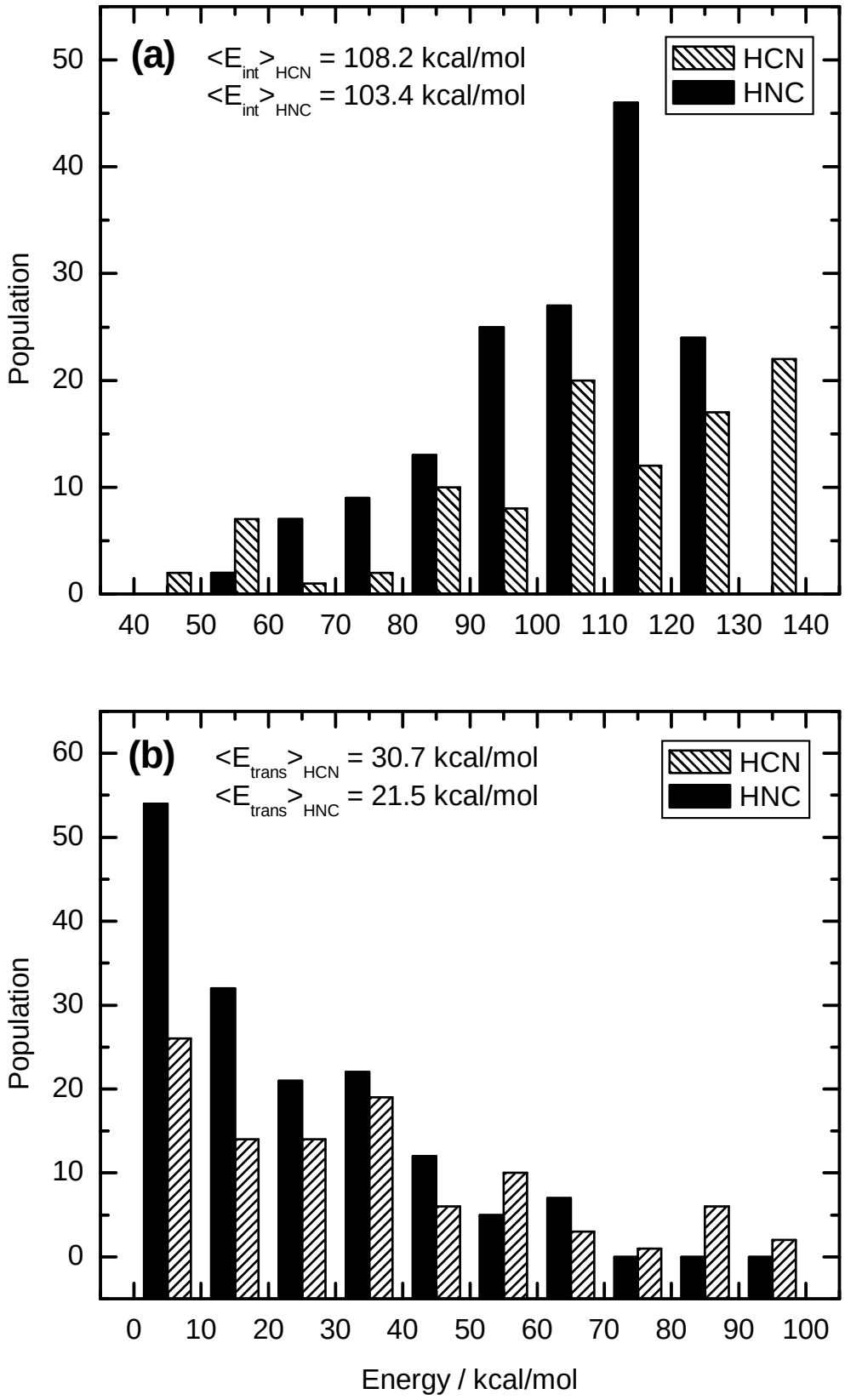
(a)
<E_int>_HCN = 108.2 kcal/mol
<E_int>_HNC = 103.4 kcal/mol
HCN
HNC
Population
0
10
20
30
40
50
40
50
60
70
80
90
100
110
120
130
140
(b)
<E_trans>_HCN = 30.7 kcal/mol
<E_trans>_HNC = 21.5 kcal/mol
HCN
HNC
Population
0
10
20
30
40
50
60
0
10
20
30
40
50
60
70
80
90
100
Energy / kcal/mol

Fig.7